Groundwater for Sustainable Development 14 (2021) 100624

Contents lists available at ScienceDirect

Groundwater for Sustainable Development

journal homepage: www.elsevier.com/locate/gsd

Research paper

Assessment of mechanical dispersion effects on mixing zone under extreme saltwater intrusion

Sugiarto Badaruddin [a,*], S. Sadjad Mehdizadeh [b]

[a] Civil Engineering Department, Politeknik Negeri Ujung Pandang, P.O. Box 90245, South Sulawesi, Indonesia
[b] Civil Engineering Department, Islamic Azad University, Central Tehran Branch, P.O. Box 13185-768, Tehran, Iran

ARTICLE INFO

Keywords:
Saltwater intrusion
Mechanical dispersion
Longitudinal dispersivity
Transversal dispersivity

ABSTRACT

The previous studies primarily identify the two types of saltwater encroachment processes like active SI (seawater intrusion) and passive SI (submarine groundwater discharge). Under passive SI, the hydraulic gradient inclines towards the sea, making density and fresh groundwater flow work in opposite directions. Under active SI, the hydraulic gradient inclines landward, and density and fresh groundwater flow work in the same direction, causing more aggressive salinization and wider mixing zones. Mechanical dispersion's effects in controlling the mixing zones in coastal aquifers have become the subject of ongoing debate in SI studies. In this study, numerical experimentations of scaled-tank and a field-scale model were used to explore the influence of longitudinal and transversal dispersivities, separately, on the width of the mixing zone under passive and active SI, in response to inland freshwater head decline. The results show that under steady SI conditions, increasing the longitudinal dispersivity value widened the lower part of the mixing zone while increasing the transversal dispersivity value increased the mixing zone's width both at the lower and the upper part of the saltwater wedge. The same phenomenon as steady-state SI results was observed for passive SI conditions even though with larger effects. While under active SI, both the increase of longitudinal and transversal dispersivities widened the width of the mixing zones but their quantitative impacts are larger compared to those in passive SI conditions. As an instance, when the transverse dispersivity is increased 50 times, the width of the mixing zone at the middle of the saltwater wedge is almost doubled compared to it in the passive case. Ultimately, it is found that under active circumstances, the shear effect of transverse dispersivity pushes the toe position back.

1. Introduction

Progressive seawater intrusion (SI) into coastal aquifers is one of the common effects of groundwater overexploitation in coastal areas (Custodio, 2002). SI is a phenomenon where seawater intrudes into a coastal aquifer and pollutes fresh groundwater resources (Bear, 2012). Mixing zones delineate the water exchange between groundwater and intruded seawater and are affected by mechanical dispersion and molecular diffusion. (Lu et al., 2009). Effective management of coastal groundwater resources usually requires a good description of the position and the thickness of the mixing zone in coastal aquifers (Abarca and Clement, 2009; Werner et al., 2013).

Previous studies have recognised two types of SI: passive and active (Bear and Dagan, 1964; Mahesha, 1995; Morgan et al., 2013). In passive SI, the positive hydraulic gradient is toward the sea and forces seawater and fresh groundwater to flow in the opposite direction. This results in the normal wedge-shaped saltwater plumes that are mostly associated with SI. In active SI, the hydraulic gradient slopes towards the land, and density and fresh groundwater flow act in the same direction, causing more destructive salinization and wider mixing zones (Werner et al., 2012; Morgan et al., 2013; Badaruddin et al., 2015, 2017).

An important and difficult parameter to assess in SI in corresponding to the mixing zone is mechanical dispersion (Abarca et al., 2004; Neupauer et al., 2020). The effect of dispersivity parameter in controlling the dispersion region has become a debatable issue in SI studies since this is assumed to control the width of mixing zones produced in SI (Zhang et al., 2002; Abarca et al., 2007). Several studies have been carried out to investigate the relationship between dispersivity parameters and the mixing zone characteristics under stable SI configurations (i.e., steady-state/passive SI), and there are very limited relevant works of literature available that focused on transient SI conditions (e.g., Ataie-Ashtiani et al., 1999; Badaruddin et al., 2017).

* Corresponding author.
E-mail addresses: sugibadaruddin@poliupg.ac.id (S. Badaruddin), Saj.Mehdizadeh@iauctb.ac.ir (S.S. Mehdizadeh).

https://doi.org/10.1016/j.gsd.2021.100624
Received 21 March 2021; Received in revised form 31 May 2021; Accepted 11 June 2021
Available online 17 June 2021

Dagan (2006) showed that under steady-state conditions, transversal dispersivity is the main factor responsible for the width of the solute mixing between freshwater and saltwater in homogeneous coastal aquifers. Several experimental investigations of SI also demonstrated that pore-scale transverse dispersion causes thin dispersion zones in SI physical models (e.g., Goswami and Clement, 2007; Abarca and Clement, 2009; Chang and Clement, 2012; Abdoulhalik and Ahmed, 2018). On the other hand, Abarca et al. (2007) showed through the numerical modelling of the benchmark Henry problem that under steady-state conditions, the contributions of longitudinal and transversal dispersivity are quantitatively similar in widening the mixing zone in coastal aquifers. They showed that an increase of longitudinal dispersivity widens the lower part of the mixing zone in which the concentration gradient and the velocity vector are parallel, while an increase of transversal dispersivity widens the mixing zone in general due to its shear effect, making the mixing zone moves seaward at the bottom and inland at the top. In the case of tidal effects, Ataie-Ashtiani et al. (1999) found that under transient passive SI conditions, both longitudinal and transversal dispersivity are essential for the configuration of the freshwater-saltwater interface but the interface shape is most sensitive to the changes in longitudinal dispersivity relative to transversal dispersivity.

Since the previous studies are mainly based on steady-state/passive SI conditions, the influence of dispersivity parameters on the zone of mixing under active SI situation has been neglected, despite some SI studies have identified the occurrence of active SI in many areas (i.e., Yakirevich et al., 1998; Fetter, 2018; Werner and Gallagher, 2006; Morgan et al., 2013). Badaruddin et al. (2015 and 2017) have shown through numerical modelling that under active SI circumstances due to an inland freshwater head decline (FHD), the width of the mixing zone at the upper region of the coastal aquifer is very critical in generating water table salinization phenomenon, particularly in shallow unconfined coastal aquifers due to its potential to salinize the unsaturated zone above aquifers through capillary rise (Werner and Lockington, 2006). Badaruddin et al. (2017) also have indicated through numerical modelling that mechanical dispersivity has a significant effect in increasing the width of the mixing zone both under passive and active SI conditions. Nonetheless, both Badaruddin et al. (2015) and (2017) did not explore further to what extent longitudinal and transversal dispersivities affect the width of the mixing zone under such conditions.

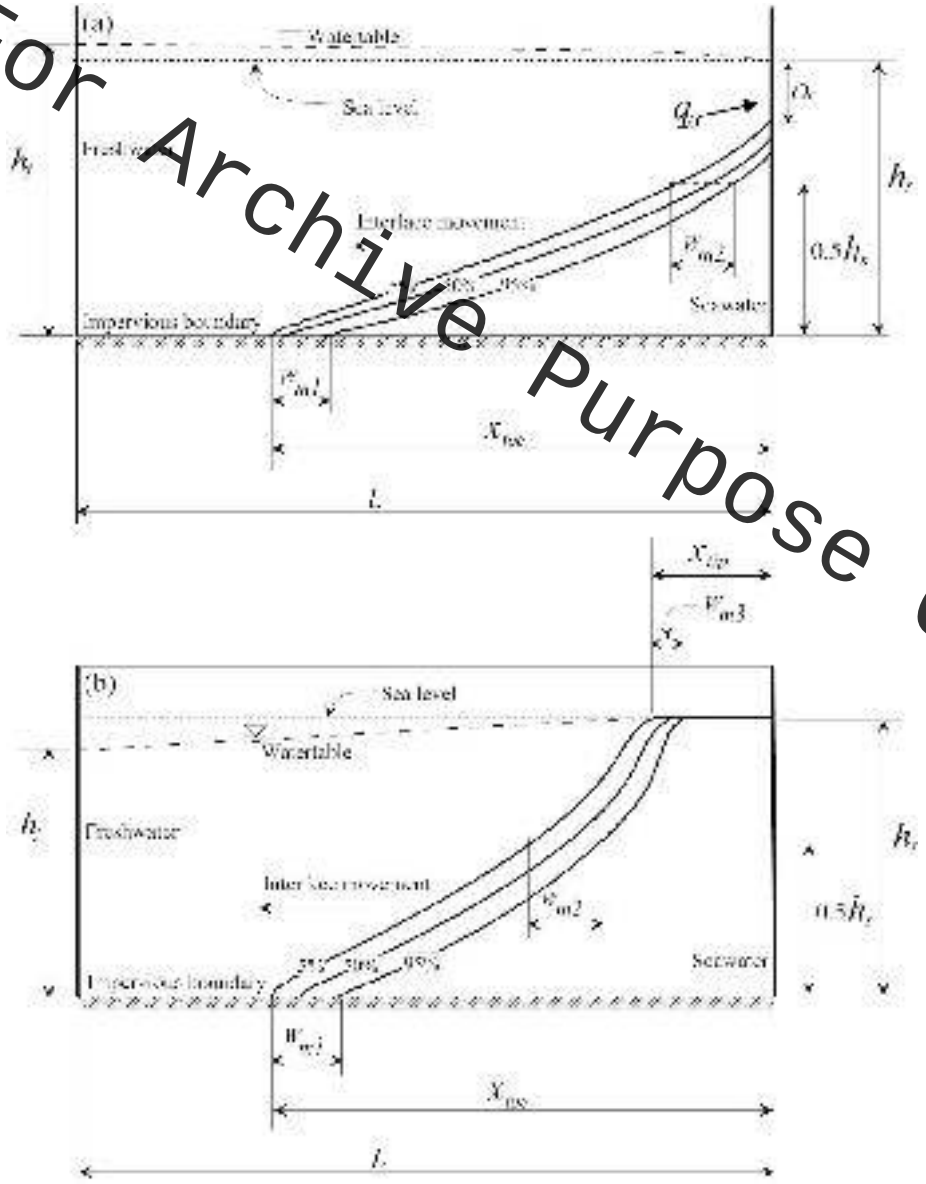

Fig. 1. Conceptual model of an unconfined coastal aquifer subjected to: (a) passive SI and (b) active SI and (modified from Badaruddin et al., 2017).

Due to the scarce of research on active SI, in this study, numerical modelling is used to undertake an investigation on the effect of longitudinal and transversal dispersivity on the width of the mixing zone under active SI, in response to an inland FHD. Intense FHD as the consequence of groundwater overexploitation is reported in previous researches (e.g. Alfarrah and Walraevens, 2018; Ochoa-González et al., 2018). FHD in stressed aquifers in association with drought may cause land subsidence (Vahidipour et al., 2021). For comparison, the effects of dispersivities on the mixing zone under passive and steady-state SI situations are also considered. This study is essential to continue the work of Werner et al. (2013), Badaruddin et al. (2015), and (2017) to provide systematic numerical experimentation in examining the individual influence of longitudinal and transversal dispersivities on the mixing zones in coastal aquifers under passive and active SI situations. This study is also beneficial in clarifying the significance of the mechanical dispersivity parameter in solute transport modelling.

2. Methodology

2.1. Conceptual model

Fig. 1 shows a schematic model of an unconfined coastal aquifer, following the conceptual case used in Badaruddin et al. (2015). Three different salinity contours were measured in evaluating the interface configuration (i.e., 5, 50, and 95% of seawater salinity), and both the 5% interface toe at the aquifer base x_{toe} [L] and the 5% interface tip at the water table x_{tip} [L] were evaluated. The horizontal length between 5% and 95% of seawater salinity contour at the aquifer base (W_{m1} [L]), at the half of the interface (W_{m2} [L]), and at the water table (W_{m3} [L]) was considered as the width of the transition zone. In Fig. 1, the right and the left sides represent the coastal and the inland boundaries, respectively, with h_s [L] the depth seawater below sea level, and h_f [L] the inland freshwater head. Moreover, q_0 is freshwater discharge to the sea [L^2/T] and O_f [L] is the freshwater/brackish water outflow face.

In examining the effect of mechanical dispersivities on the mixing zone under passive and active SI, the 2D model domain of a scaled-tank was first considered. Parameters of the scaled-tank model follow an SI experimental study presented by Badaruddin et al. (2015). The FHD experiment in their study was carried out by a tank with 52 mm width filled by natural sand. In their work, the interface was first established as a steady-state condition and then an instantaneous inland FHD of Δh_f [L] causes the interface to move landward. In their study, the steady-state conditions were confirmed after 4 h where h_f and h_s were maintained at 50.4 cm and 48.2 cm, respectively (refer to Fig. 1). Passive SI in response to an FHD was induced by dropping h_f from 50.4 to 49.4 cm instantaneously (refer to Fig. 1) and passive SI was run for 210 min. To induce active SI, h_f was instantaneously dropped from 49.4 to 43.4 cm (i.e. below the h_s: refer to Fig. 1) and active SI was run for 18 min. All the parameters for the scaled-tank model are measured and summarized in Table 1. The measurement process of soil and fluid characteristics is provided by Badaruddin et al. (2015) and is not stated here for brevity.

Table 1
Parameter values for the scaled-tank model.

Parameter	Variable	Value
Domain length (m)	L	1.17
Domain height (m)	H	0.52
Domain width (m)	W	0.05
Hydraulic conductivity (m/d)	K	269
Initial inland freshwater head (m)	h_{f0}	0.504
Post-inland freshwater head 1 (m)	h_{f1}	0.494
Post-inland freshwater head 2 (m)	h_{f2}	0.434
Seawater level (m)	h_s	0.482
Porosity (−)	n	0.4
Specific yield (−)	S_y	0.32
Longitudinal dispersivity (m)	α_L	0.004
Transversal dispersivity (m)	α_T	0.0004
Molecular diffusion (m^2/d)	D_m	8.64×10^{-5}
Seawater density (kg/m^3)	ρ_s	1018.3
Freshwater density (kg/m^3)	ρ_f	998.1
Sea concentration (kg/m^3)	C_s	26.4

2.2. Numerical model

In this study, numerical experimentations were conducted using the variable-density groundwater flow and transport code SEAWAT version 4 (Langevin et al., 2008), which is commonly used and has been validated using some benchmarks (Brovelli et al., 2007; Goswami and Clement, 2007). For each steady-state simulation, specified-head boundary conditions were used at the left and the right sides of the model, and the base of the domain was prescribed no-flow conditions. The right sea boundary represents seawater hydrostatic conditions, whereas a constant freshwater head was applied at the inland boundary. A steady-state condition was used in transition simulations as an initial condition.

In order to meet the accuracy and convergence requirement for grid spacing in the model, the mesh Peclet number (Pe_m) (Voss and Souza, 1987; Zhang et al., 2002; Brovelli et al., 2007) was used to specify the discretization of the model domain:

$$Pe_m = \frac{\Delta L}{\alpha_L} < 4 \quad (1)$$

where ΔL [L] is the grid spacing. Following Badaruddin et al. (2015), for the scaled-tank model, a uniform grid size of $\Delta x = 0.50$ cm and $\Delta z = 0.25$ cm was used, resulted in a grid of 48,672 cells and a Pe of 1.25. A time step of 30 s was employed, and the transport step size was set to 3 s. Three stress periods were defined in the numerical model of the sand-tank scale model, as: (1) a 4-h period to reach steady-state conditions with h_s at 48.2 cm and h_f at 50.4 cm (refer to Fig. 1), (2) h_f was dropped by 1.0 cm instantaneously, and passive SI was simulated for 210 min, and (3) h_f was dropped instantaneously by 6.0 cm to produce active SI for 18 min.

Following Abarca et al. (2007), different ratios of longitudinal dispersivity (α_L [L]) to transversal one (α_T [L]) according to Table 2 were introduced in the numerical experiments, representing the individual increase of α_L (i.e., 20, 90, and 150 times): and α_T (i.e., 2, 1, and 0.2 times) to realize the effect of longitudinal and transversal dispersivity parameters independently on the mixing zones.

3. Results and discussion

3.1. Steady-state SI conditions

Fig. 2 (a, b, and c) compare the salinity distribution of Case 1 with Cases 2, 3, and 4 under steady-state SI conditions. Cases 2, 3, and 4 represent the increase of α_L by 2, 3, and 5 times, respectively, relative to the α_L of Case 1. The figure shows that the length of x_{toe}, x_{tip}, W_{m1}, W_{m2}, and W_{m3} is 26.7, 0, 3.5, 5.3, and 0 cm, respectively. These results are in accordance with the results of Badaruddin et al. (2015). The results demonstrate that the value of x_{toe} (26.7 cm) and x_{tip} (0 cm) are constant for these cases, but there are slight variations observed on the width of the mixing zones, particularly at W_{m1} and W_{m2}. For example, increasing α_L by 5 times changed the values of W_{m1} from 3.5 cm in Case 1–8.2 cm in Case 4 (almost doubled) and W_{m2} from 5.3 cm in Case 1–6.3 cm in Case 4. From Fig. 2, it is clear that under steady-state SI conditions, increasing longitudinal dispersivity by 5 times will widen the lower part of the mixing zone by 130%. The line of 5% salinity remained static but the mixing zones broaden seaward and downward.

Fig. 3 (a, b, and c) present the comparison of salinity distribution between Case 1 and Cases 5, 6, and 7. Cases 5, 6, and 7 represent the increase of α_T by 5, 10, and 50 times, respectively, compared to the α_T used in Case 1. The figures present that in general, the x_{toe} values are

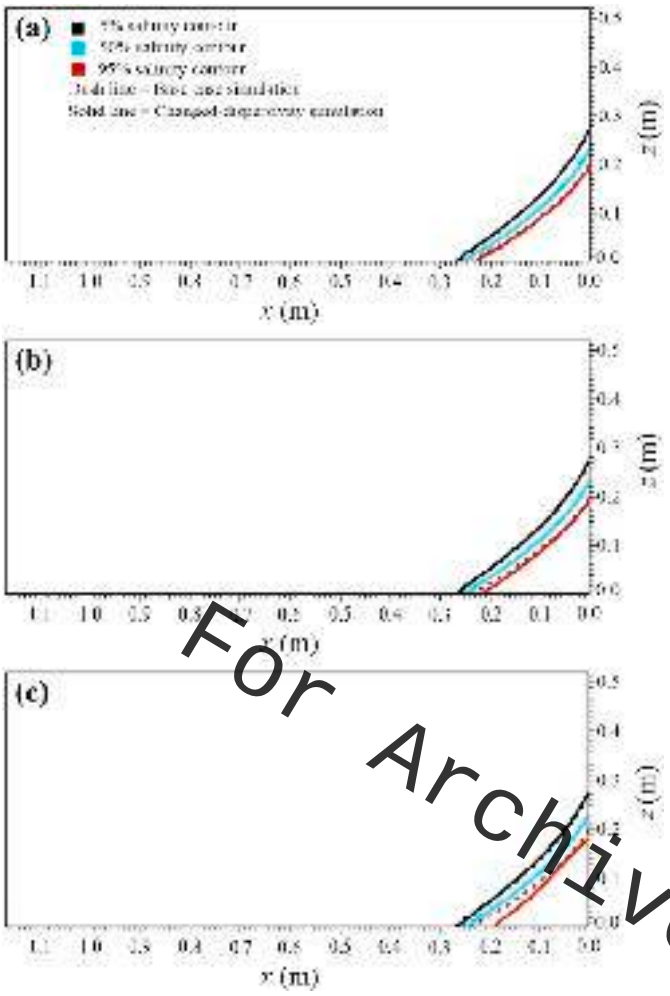

Fig. 2. Comparison of salinity distribution between Case 1 (base case 1) with (a) Case 2 (b) Case 3, and (c) Case 4 under steady-state SI.

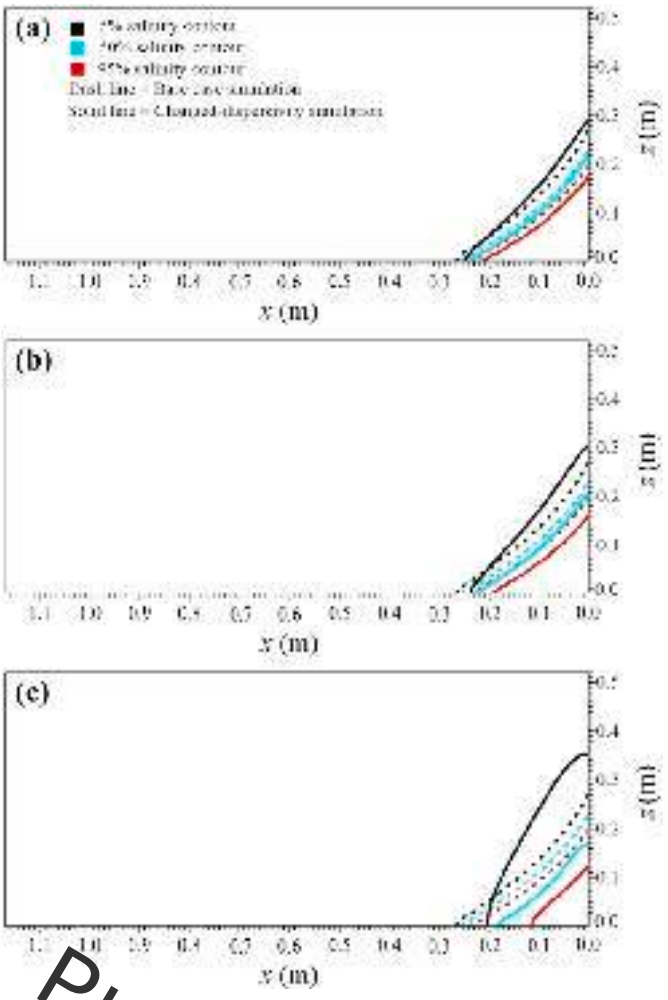

Fig. 3. Comparison of salinity distribution between Case 1 (base case 1) and (a) Case 5 (b) Case 6, and (c) Case 7 under steady-state SI.

Table 2
Mechanical dispersivity parameters for all simulations.

Simulation	Parameter	
	α_L (m)	α_T (m)
Case 1 (base case 1) (steady) (Scaled-tank model)	0.004	0.0004
Case 2 (steady)	0.008	0.0004
Case 3 (steady)	0.012	0.0004
Case 4 (steady)	0.02	0.0004
Case 5 (steady)	0.004	0.002
Case 6 (steady)	0.004	0.004
Case 7 (steady)	0.004	0.02
Case 8 (base case 2) (passive SI) (Scaled-tank model)	0.004	0.0004
Case 9 (passive SI)	0.008	0.0004
Case 10 (passive SI)	0.012	0.0004
Case 11 (passive SI)	0.02	0.0004
Case 12 (passive SI)	0.004	0.002
Case 13 (passive SI)	0.004	0.004
Case 14 (passive SI)	0.004	0.02
Case 15 (base case 3) (active SI) (Scaled-tank model)	0.004	0.0004
Case 16 (active SI)	0.008	0.0004
Case 17 (active SI)	0.012	0.0004
Case 18 (active SI)	0.02	0.0004
Case 19 (active SI)	0.004	0.002
Case 20 (active SI)	0.004	0.004
Case 21 (active SI)	0.004	0.02
Case 22 (base case) (Field-scaled model)	1	0.1
Case 23	0.1	0.01
Case 24	10	1

decreased and the width of the mixing zones are increased with the increase of α_T. The x_{toe} values in Cases 5, 6, and 7 are 24.9 cm, 23.5 cm, and 20.2 cm, respectively. The length of x_{tip} is zero in these cases, except for Case 7 where the x_{tip} is 2.1 cm. These results imply that an increase of transversal dispersivity widened the width of the mixing zones in all parts of the saltwater wedge but its shear effect drove the mixing zone at the bottom to move backward and landward at the top. This potentially increases salinization at the water table.

3.2. Passive SI conditions

Fig. 4 (a, b, and c) compare the salinity distributions between Case 8 and Cases 9, 10, and, 11. Cases 9, 10, and 11 represent the increase of α_L by 2, 3, and 5 times, respectively. The salinity distribution under transient passive SI condition for Case 8 (base case 2) is depicted in Fig. 4a. As the figure presents the x_{toe}, x_{tip}, W_{m1}, W_{m2} and W_{m3} are 59, 0, 7.1, 10.22, and 0 cm, respectively. These results are the same as the results of Badaruddin et al. (2015). The results demonstrate that the values of x_{tip} (0 cm) and W_{m3} (0 cm) are constant for these cases, but there are slight changes noticed on x_{toe} and the width of the mixing zones, particularly at W_{m1} and W_{m2}. Raising α_L by 5 times increased the values of W_{m1} from 7.1 cm in Case 8–15.7 cm in Case 11 (almost doubled) and W_{m2} from 10.2 cm in Case 8–17 cm in Case 11 (67% increase). On the contrary, decreasing the x_{toe} from 59 cm in Case 8–55 cm in Case 11. The same phenomenon was observed between steady-state and passive SI conditions where increasing the α_L y may widen the lower part of the mixing

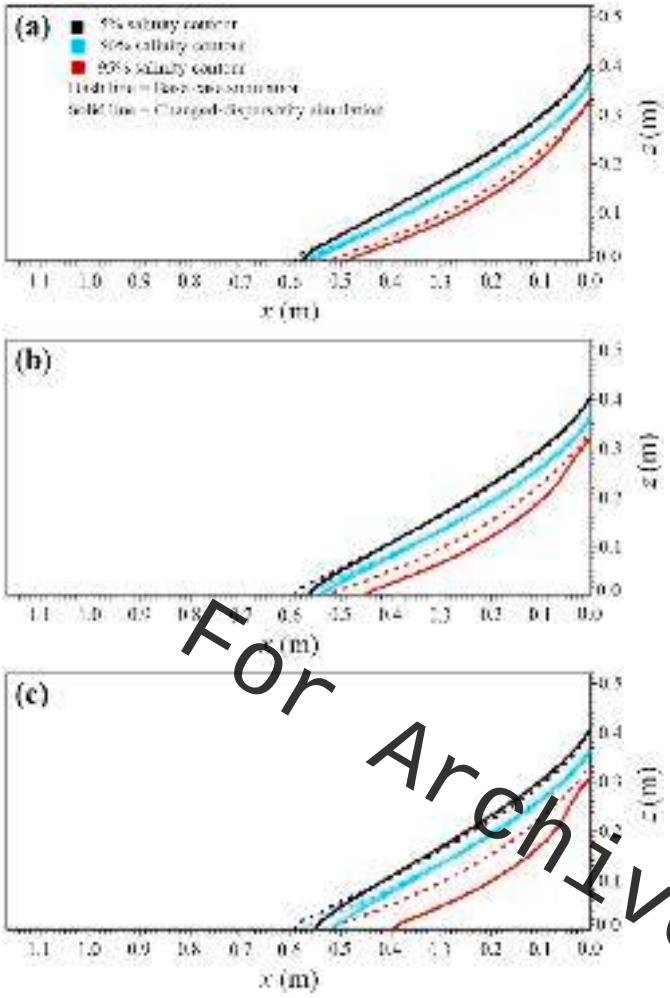

Fig. 4. Comparison of salinity distribution between Case 8 (base case 2) and (a) Case 9 (b) Case 10, and (c) Case 11 at 210 min after steady-state condition.

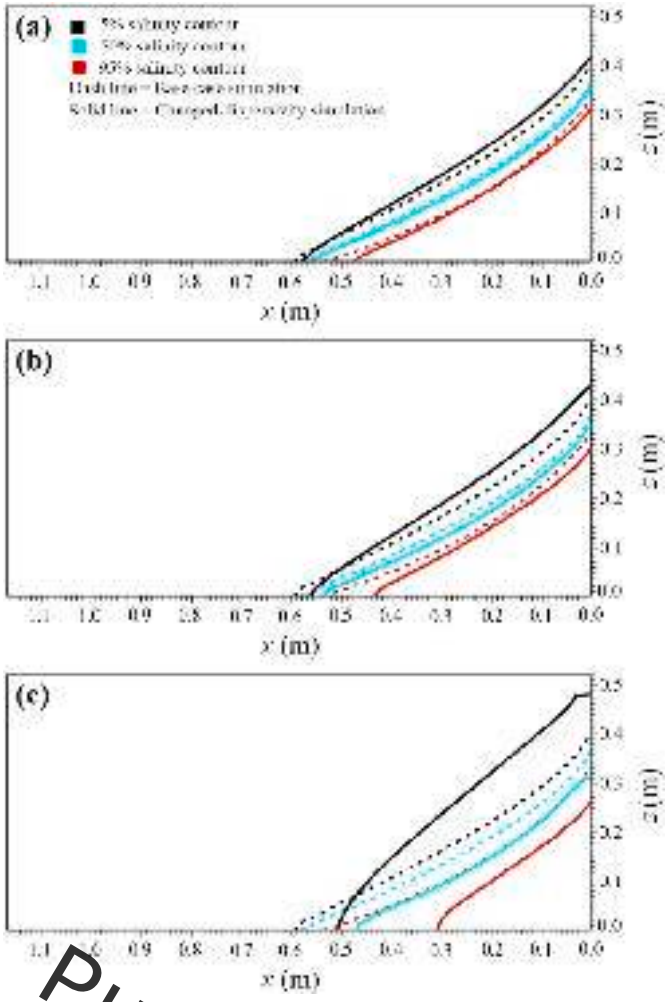

Fig. 5. Comparison of salinity distribution between Case 8 (base case 2) and (a) Case 12 (b) Case 13, and (c) Case 14 at 210 min after steady-state condition.

zone. However, a tiny difference in response was detected. Under transient passive SI, the lower part of the 5% salinity contour was pushed back slightly seaward whereas the mixing zone still broadened seawards and downwards.

Fig. 5 (a, b, and c) present the comparison of salinity distribution between Case 8 (base case 2) and Cases 12, 13 and 14. Cases 12, 13, and 14 denote the increase of α_T by 5, 10, and 50 times, respectively, compared to the α_T in Case 8. The figure shows that in general, the x_{toe} values are decreased and the width of the mixing zones are increased with the increase of α_T, similar to the results of steady-state SI. The x_{toe} values in Cases 12, 13, and 14 are 57.9 cm, 56.5 cm, and 50.9 cm, respectively. The length of x_{tip} is also zero in these cases, except for Case 14 where the x_{tip} is 3.5 cm. These results imply that an increase of transversal dispersivity under passive SI widened the width of the mixing zones in both the lower and the upper part of the saltwater wedge and increased the slope of salinity contours. This also potentially increases salinization at the water table.

3.3. Active SI conditions

Fig. 6 (a, b, and c) compare the salinity distribution of Case 15 (base case 3) with Cases 16, 17, and 18. Cases 16, 17, and 18 represent the increase of α_L by 2, 3, and 5 times, respectively, relative to the α_L of Case 15. Fig. 6a shows that the values of x_{toe}, x_{tip}, W_{m1}, W_{m2}, and W_{m3} are 87.5, 14.6, 16.9, 17.1, and 9.8 cm, respectively. These results are in agreement with the results of Badaruddin et al. (2015). The results show that the value of x_{toe} and x_{tip} are slightly modified for these cases but there are significant changes noted on the width of the mixing zones. Increasing α_L by 5 times changed the values of x_{toe} from 87.5 cm in Case 15–99 cm (13% increase) in Case 18 and x_{tip} from 14.6 cm to 22 cm (1.5 times). The values of W_{m1} are also changed from 16.9 cm in Case 15–36.2 cm in Case 18 (214% increase), W_{m2} from 17.1 cm to 34.3 (doubled) cm, and W_{m3} from 9.8 cm to 22.4 cm (2.3 times). From Fig. 6, it is obvious that under active SI conditions, increasing α_L widened the mixing zone both at the lower and upper part of the wedge, albeit the upper part was more sensitive to the change. This potentially increases salinization at the water table. The performance of the mixing zone in this condition is different from the previous results in steady-state and passive SI. Here all parts of 5% and 95% salinity contours were pushed inland and seaward respectively which results in the broad mixing zone.

Fig. 7 (a, b, and c) provide the comparison of salinity distribution between Case 15 (base case 3) and Cases 19, 20, and 21. The values of α_T increased by 5, 10, and 50 times in Cases 19, 20, and 21, respectively. The figures show that in general, the values of x_{toe} decreased and the x_{tip} increased with the increase of α_T. In Cases 19, 20, and 21, the x_{toe} values are 83.5 cm, 81.5 cm, and 74.5 cm, respectively and the x_{tip} values are 16.1 cm, 18.2 cm, and 29 cm. The widths of the mixing zones are increased with the increase of α_T. These results imply that under active SI conditions, an increase of α_T widened the mixing zones in all parts of the interface but in a different fashion compared to the change of longitudinal dispersivity. At this condition, the shear effect of transversal dispersivity becomes more obvious, pushing the mixing zone backward

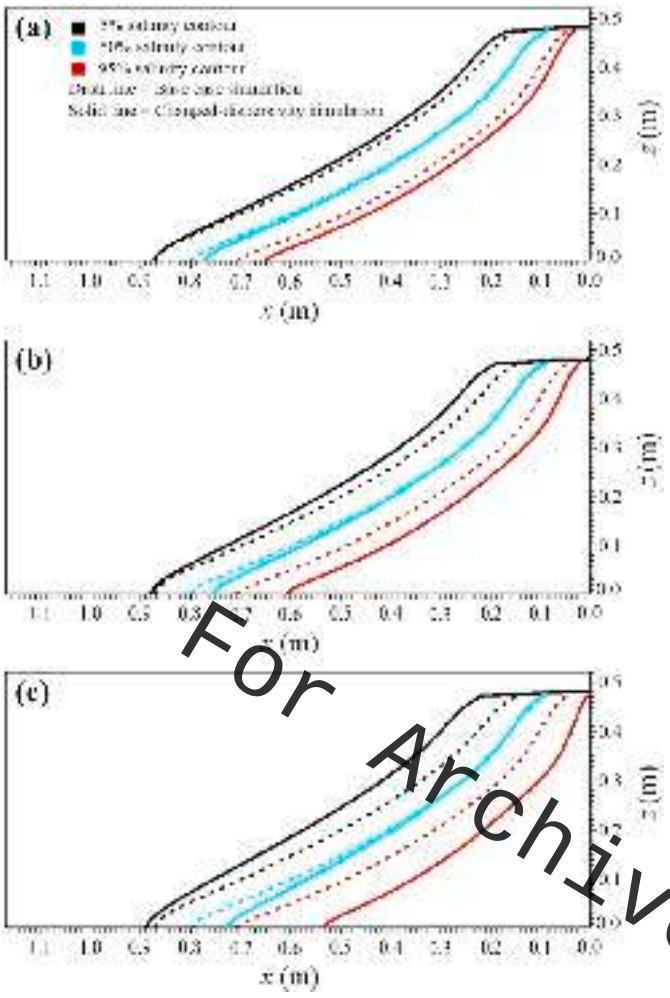

Fig. 6. Comparison of salinity distribution between Case 15 (base case 3) and (a) Case 16 (b) Case 17, and (c) Case 18 at 220 min after steady-state condition (10 min after passive simulation).

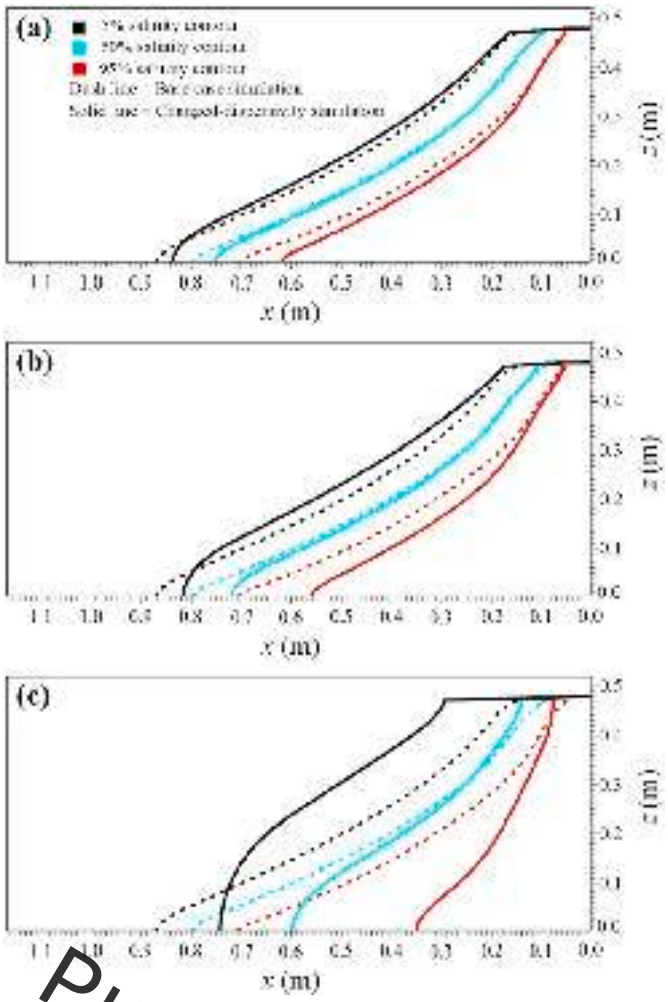

Fig. 7. Comparison of salinity distribution between Case 15 (base case 3) and (a) Case 19 (b) Case 20, and (c) Case 21 at 220 min after steady-state condition (10 min after passive simulation).

at the bottom and landward at the top which is also potentially increasing salinization at the water table.

3.4. Field-scale model

Fig. 8 provides the comparison of salinity distribution between a field base case and the cases with low and high dispersivities. This result is taken from Badaruddin et al. (2017) to confirm the results obtained in this study. Aside from the type of aquifer which is unconfined, the geometry of the coastal aquifer and the values of hydrologic parameters used in the field base case of the study mainly followed those in Lu and Werner (2013). The length of aquifer L [L] was 1000 m with h_s of 30 m. The coastal aquifer was assumed as homogeneous isotropic with a hydraulic conductivity K [L/T] of 10 m/d, and an effective porosity n [−] of 0.3. Seawater and freshwater densities were 1025 kg/m^3 and 1000 kg/m^3, respectively. 35 kg/m^3 salt concentration was considered for seawater boundary. For the base case, the longitudinal dispersivity was 1 m and the transverse dispersivity was one-tenth of α_L (Lu and Werner, 2013; Abarca et al., 2007). Following Jakovovic et al. (2011), a molecular diffusivity D_m [L^2/T] of 8.64 × 10^{-5} m^2/d was adopted.

Fig. 8 shows the effect of modifying dispersivity on active SI. It can be seen that higher dispersion values (increasing both a_L and a_T) led to rates of interface movement that were lower at the toe but higher at the tip (thereby increasing the saltwater wedge steepness), and resulted in mixing zone widths that were larger both at the toe and tip. These results are in good agreement with the results gained in Cases 15 to 18. This is also consistent with the steady-state SI findings of Kerrou and Renard (2010), who found that stronger dispersion leads to decreased density contrasts due to the wider mixing zone. This condition causes rotation of the mixing zone alignment such that the interface toe moves seaward relative to the interface tip.

4. Conclusion

In this research work, the individual effect of mechanical dispersivities (i.e., longitudinal and transversal) on the freshwater-saltwater interface profile was investigated using numerical model of SEAWAT. The results of this study highlight the role of these two parameters in shaping the extent of seawater intrusion especially under active state which was not studied in detail at the previous works of literature. Based on the results of numerical modelling, the individual effect of longitudinal and transversal dispersivities on mixing zone's profile under steady-state SI are in accordance with the results of previous studies. Under steady-state SI conditions, an increase of longitudinal dispersivity widens the lower part of the mixing zone while an increase of transversal dispersivity widens the mixing zone in all part of the saltwater wedge and the same phenomenon was observed on the results of transient passive SI conditions. Under transient active SI condition, both an increase of longitudinal and transversal dispersivities may increase the width of the mixing zones in all part of the freshwater-

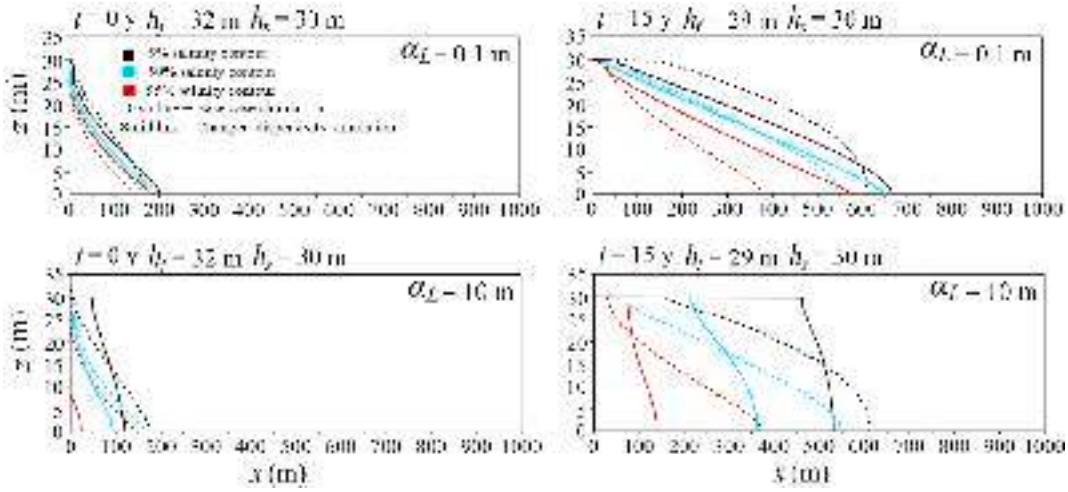

Fig. 8. Comparison of salinity distribution between field base case (Case 22) and Case 23 (a_L = 0.1 & a_T = 0.01 m) and Case 24 (a_L = 10 & a_T = 1 m).

saltwater interface but in different fashion. This implies that both longitudinal and transversal dispersivity are significantly important in controlling the width of the mixing zone and each of this parameter cannot be neglected in numerical model. The result of this research is useful as guidance in solute transport modelling, at least to identify the effect of mechanical dispersion involved in affecting the results of numerical modelling.

Declaration of competing interest

The authors declare that they have no known competing financial interests or personal relationships that could have appeared to influence the work reported in this paper.

Acknowledgements

The authors wish to thank anonymous reviewers for their constructive suggestions.

References

Abarca, E., Carrera, J., Held, R., Sánchez-Vila, X., Dentz, M., Kinzelbach, W., Vázquez-Suné, E., 2004. Effective dispersion in seawater intrusion through heterogeneous aquifers. Groundwater Saline Intrus. (15), 49.
Abarca, E., Carrera, J., Sánchez-Vila, X., Dentz, M., 2007. Anisotropic dispersive Henry problem. Adv. Water Resour. 30 (4), 913–926.
Abarca, E., Clement, T.P., 2009. A novel approach for characterizing the mixing zone of a saltwater wedge. Geophys. Res. Lett. 36 (6).
Abdoulhalik, A., Ahmed, A.A., 2018. Transience of seawater intrusion and retreat in response to incremental water-level variations. Hydrol. Process. 32 (17), 2721–2733.
Alfarrah, N., Walraevens, K., 2018. Groundwater overexploitation and seawater intrusion in coastal areas of arid and semi-arid regions. Water 10 (2), 143.
Ataie-Ashtiani, B., Volker, R.E., Lockington, D.A., 1999. Tidal effects on sea water intrusion in unconfined aquifers. J. Hydrol. 216 (1–2), 17–31.
Badaruddin, S., Werner, A.D., Morgan, L.K., 2015. Water table salinization due to seawater intrusion. Water Resour. Res. 51 (10), 8397–8408.
Badaruddin, S., Werner, A.D., Morgan, L.K., 2017. Characteristics of active seawater intrusion. J. Hydrol. 551, 632–647.
Bear, J., Dagan, G., 1964. Moving interface in coastal aquifers. J. Hydraul. Div. 90 (4), 193–216.
Bear, J., 2012. Hydraulics of Groundwater. Courier Corporation.
Brovelli, A., Mao, X., Barry, D.A., 2007. Numerical modeling of tidal influence on density-dependent contaminant transport. Water Resour. Res. 43 (10).
Chang, S.W., Clement, T.P., 2012. Experimental and numerical investigation of saltwater intrusion dynamics in flux-controlled groundwater systems. Water Resour. Res. 48 (9).
Custodio, E., 2002. Aquifer overexploitation: what does it mean? Hydrogeol. J. 10 (2), 254–277.
Dagan, G., 2006. Transverse mixing at fresh-water sea-water interfaces: an unresolved issue. In: 1st SIM-SICA—First International Joint Sea Water Intrusion Conference (19th Seawater Intrusion Meeting/3rd Seawater Intrusion in Coastal Aquifers), Automated Time-Lapse Electrical Resistivity Tomography (ALERT), Cagliari, Italy.
Fetter, C.W., 2018. Applied Hydrogeology. Waveland Press.
Goswami, R.R., Clement, T.P., 2007. Laboratory-scale investigation of saltwater intrusion dynamics. Water Resour. Res. 43 (4).
Jakovovic, D., Werner, A.D., Simmons, C.T., 2011. Numerical modelling of saltwater upconing: comparison with experimental laboratory observations. J. Hydrol. 402 (3–4), 261–273.
Kerrou, J., Renard, P., 2010. A numerical analysis of dimensionality and heterogeneity effects on advective dispersive seawater intrusion processes. Hydrogeol. J. 18 (1), 55–72.
Langevin, C.D., Thorne Jr., D.T., Dausman, A.M., Sukop, M.C., Guo, W., 2008. SEAWAT Version 4: A Computer Program for Simulation of Multi-Species Solute and Heat Transport (No. 6-A22). Geological Survey (US).
Lu, C., Kitanidis, P.K., Luo, J., 2009. Effects of kinetic mass transfer and transient flow conditions on widening mixing zones in coastal aquifers. Water Resour. Res. 45 (12).
Lu, C., Werner, A.D., 2013. Timescales of seawater intrusion and retreat. Adv. Water Resour. 59, 39–51.
Mahesha, A., 1995. Parametric studies on the advancing interface in coastal aquifers due to linear variation of the freshwater level. Water Resour. Res. 31 (10), 2437–2442.
Morgan, L.K., Werner, A.D., Jakovic, K.M., Carey, H., Sundaram, B., 2013. A national-scale vulnerability assessment of seawater intrusion: first-order assessment of seawater intrusion for 12 national case study sites, Record 2013/19, Geoscience Australia, Canberra, and National Centre for Groundwater Research and Training (Adelaide).
Neupauer, R.M., Sather, L.J., Mays, D.C., Fridley, J.P., Roth, E.J., 2020. Contributions of pore-scale mixing and mechanical dispersion to reaction during active spreading by radial groundwater flow. Water Resour. Res. 56 (7), e2019WR026276.
Ochoa-González, G.H., Carreón-Freyre, D., Franceschini, A., Cerca, M., Teatini, P., 2018. Overexploitation of groundwater resources in the faulted basin of Querétaro, Mexico: a 3D deformation and stress analysis. Eng. Geol. 245, 92–106.
Vahidipour, M., Raeisi, E., Van Der Zee, S.E., 2021. Active saltwater intrusion of shrinking Bakhtegan-Thask Lakes in South Iran threatens the freshwater resources of coastal aquifers. J. Hydrol.: Reg. Stud. 34, 100790.
Voss, C.I., Souza, W.R., 1987. Variable density flow and solute transport simulation of regional aquifers containing a narrow freshwater-saltwater transition zone. Water Resour. Res. 23 (10), 1851–1866.
Werner, A.D., Gallagher, M.R., 2006. Characterisation of sea-water intrusion in the Pioneer Valley, Australia using hydrochemistry and three-dimensional numerical modelling. Hydrogeol. J. 14 (8), 1452–1469.
Werner, A.D., Ward, J.D., Morgan, L.K., Simmons, C.T., Robinson, N.I., Teubner, M.D., 2012. Vulnerability indicators of sea water intrusion. Groundwater 50 (1), 48–58.
Werner, A.D., Bakker, M., Post, V.E., Vandenbohede, A., Lu, C., Ataie-Ashtiani, B., Simmons, C.T., Barry, D.A., 2013. Seawater intrusion processes, investigation and management: recent advances and future challenges. Adv. Water Resour. 51, 3–26.
Yakirevich, A., Melloul, A., Sorek, S., Shaath, S., Borisov, V., 1998. Simulation of seawater intrusion into the Khan Yunis area of the Gaza Strip coastal aquifer. Hydrogeol. J. 6 (4), 549–559.
Zhang, Q., Volker, R.E., Lockington, D.A., 2002. Experimental investigation of contaminant transport in coastal groundwater. Adv. Environ. Res. 6 (3), 229–237.